Figure S1: Raw and filtered traces are anti-correlated and KA activity shows a shift in the theta band. Example traces are taken from the activity shown in Figs. 2A and B in the main part of the manuscript. (A) 1 s cutout of control activity from MEC (raw: black, 4-8 Hz: gray) and DG (raw: red, 4-8 Hz: orange). The traces are anti-correlated but synchronized in the theta band. (B) Same as A with same scalebars for an EA-free trace from a KA mouse. Traces are also anti-correlated, but in contrast to the control case, theta band activity in the MEC lags behind theta band activity in the DG. This especially holds true for high amplitude theta activity (black arrows).
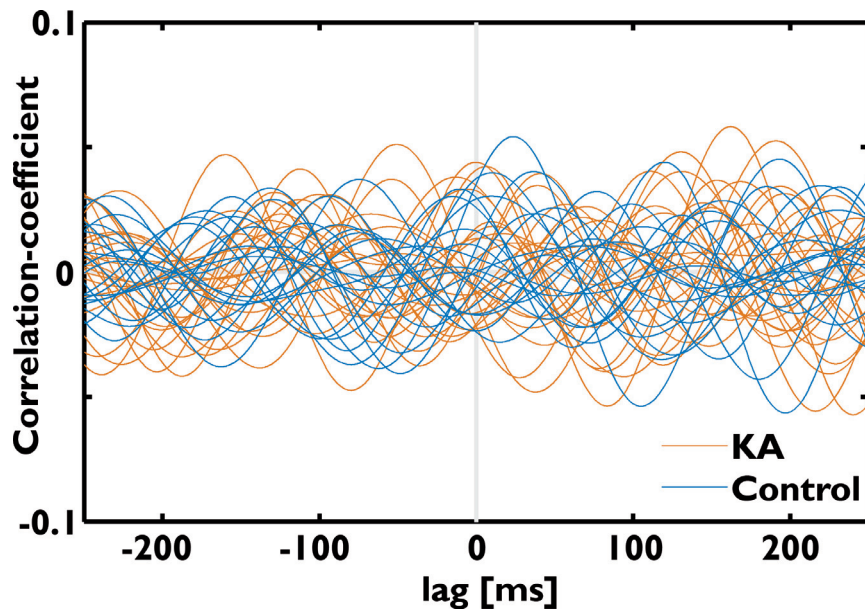
Figure S2: No lag and low correlation after shuffling of 2 s cutouts. Mean of the correlation from all epochs from one recording session for KA (K116, orange) and control example (S120, blue) from Fig. 2C after shuffling the 2 s cutouts from the filtered MEC signal. Note the different y-axis scaling from Fig. 2C, and the vanished difference regarding Δt_{peak} between KA and control.
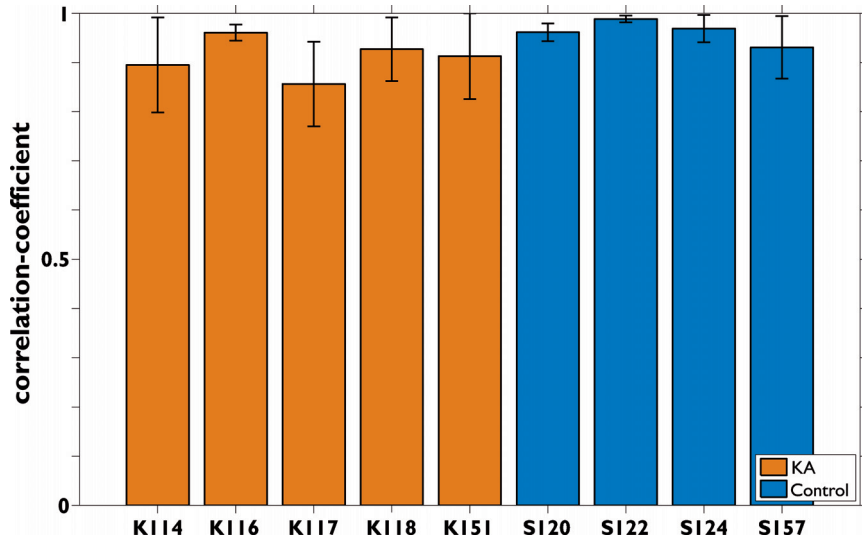
Figure S3: Δt_{peak} values are stable across weeks in both animal groups. Each bar represents the mean and the standard deviation of the average correlation coefficients of all recordings per mouse as shown for two examples in Fig. 2D in the main text. In both animal groups, the correlation results were stable across time.
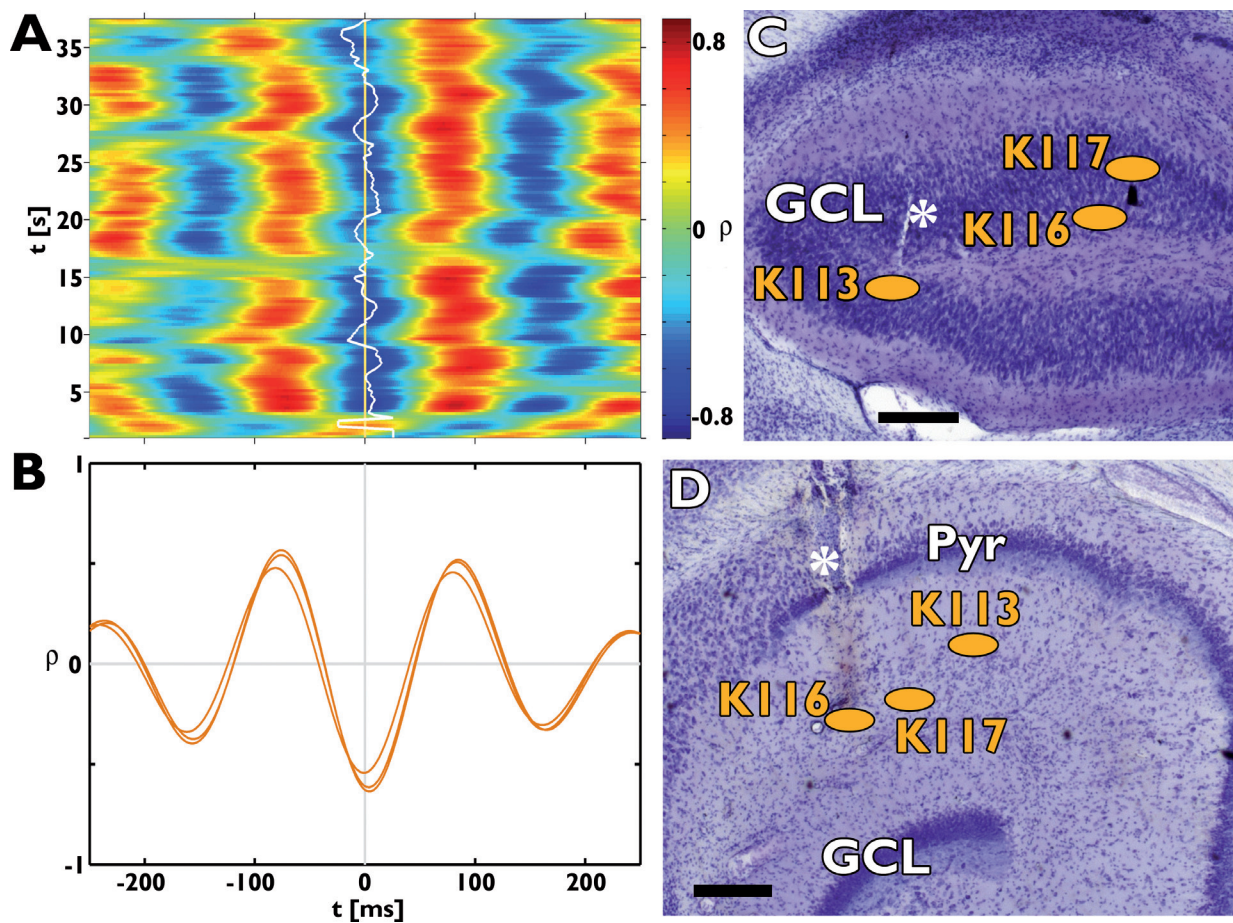
Figure S4: CA1 appears synchronized with the DG in KA mice. (A) Example of a TRCC in theta band taken from mouse K113 with electrodes in DG and intermediate CA1. The highest correlation values are close to $0\,\mathrm{ms}$ lag, suggesting that in contrast to the MEC and DG relation, DG and intermediate CA1 are synchronized. (B) Mean of all correlation values in the theta band from all recordings from KA mice with electrodes in CA1 and DG, confirming that all three mice show a Δt_{peak} around $0\,\mathrm{ms}$ lag. Note the anti-correlation between these structures, similar to the MEC-DG relation in the main text. (C) Electrode positions for DG electrodes, superimposed on a Nissl-stained slice (K113, scale bar is $200\,\mu\mathrm{m}$, Pyr = stratum pyramidale). (D) Same as C but for electrode positions in CA1, superimposed on a slice from K116. Two positions could be reconstructed in the stratum lacunosum moleculare, one in the stratum radiatum of CA1. Note, that at this intermediate hippocampal recording positions no cell loss nor granule cell dispersion appear because of the distance to the injection site in the septal DG.
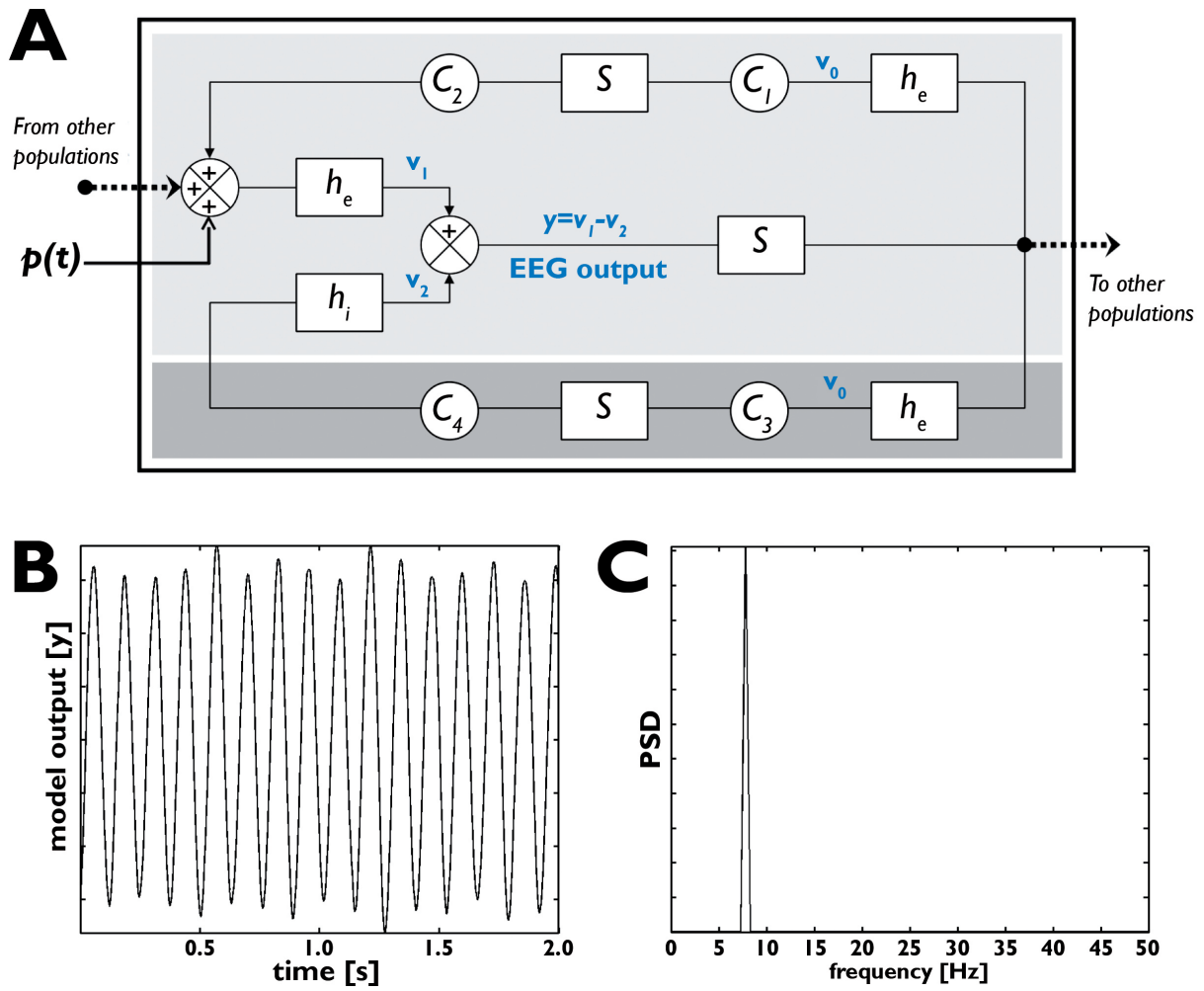
Figure S5: The Jansen model of coupled neuronal populations. (A) Block diagram of the neuronal population model. (B) Example of a simulated signal (LFP), for an oscillatory activity in theta band. (C) Power spectral density (PSD) of the simulated signal in B.

The Jansen Model of Coupled Neuronal Populations

In our computer simulations, we used Jansen's neural mass model of coupled neuronal populations (Jansen and Rit, 1995). In this model, a neuronal population contains two subpopulations, the excitatory pyramidal cells and inhibitory interneurons, connected with each other via excitatory and inhibitory synaptic connections. According to the neural mass modeling approach, each subpopulation is described by its average membrane potential (ν) and mean firing rate (m). In each subpopulation, the action of the synapses is described by a linear operator h that transforms m into ν, while the action of the neurons is modeled by a static nonlinear operator S that relates ν to m. The operator h is represented by a second-order lowpass filter with an impulse response given by $h_e(t) = Aat.u(t).e^{-at}$ for the excitatory case, and $h_i(t) = Bbt.u(t).e^{-bt}$ for the inhibitory case, where u is the Heaviside function. Parameters A and B determine the maximum amplitude of the average excitatory and inhibitory PSPs, and a and b represent the associated average rate constants (reciprocal of the time constants) of these PSPs. The operator S is described by the sigmoid function $S(\nu) = \frac{2e_0}{[1+e^{r(\nu_0-\nu)}]}$, where $2e_0$ is the maximum firing rate, ν_0 is the PSP corresponding to a firing rate e_0, and r is the steepness of the sigmoid. Synaptic interactions between pyramidal cells and inhibitory interneurons are characterized by four connectivity constants C_i, which account for the average numbers of synaptic contacts between the subpopulations. Finally, the neuronal population model is driven by a Gaussian noise input p, which represents the non-specific excitatory input from neighboring or more distant populations. The Jansen model is summarized in Fig. 5A in the main text and Fig. S5A in the supporting information.

Furthermore, multiple neuronal population models can be considered and connected to each other. Inter-population coupling is modeled by excitatory connections between the pyramidal cell subpopulations (Jansen and Rit, 1995; Wendling et al., 2000). In this study, we considered a system of $N = 2$ coupled neuronal populations (main text Fig. 5A). Two gain constants, K_{12} and K_{21}, are used to characterize the strength of the connection from population 1 to population 2, and from population 2 to population 1, respectively. The connection delays are modeled by using linear operators h_d. For simplicity, h_d function was chosen similar to h_e function, i.e. $h_d(t) = Aat.u(t).e^{-at}$.

Each neuronal population model is described by the following set of eight differential equations (see Jansen and Rit (1995); Wendling et al. (2000) for details):

$$
\begin{cases}
\dot{\nu}_0^i(t) = \nu_3^i(t) \\
\dot{\nu}_3^i(t) = A^i a^i S[\nu_1^i(t) - \nu_2^i(t)] - 2a^i \nu_3^i(t) - (a^i)^2 \nu_0^i(t) \\
\dot{\nu}_1^i(t) = \nu_4^i(t) \\
\dot{\nu}_4^i(t) = A^i a^i [p^i(t) + \sum_{j \neq i} K_{ji} \nu_6^j(t) + C_2^i S[C_1^i \nu_0^i(t)]] - 2a^i \nu_4^i(t) - (a^i)^2 \nu_1^i(t) \\
\dot{\nu}_2^i(t) = \nu_5^i(t) \\
\dot{\nu}_5^i(t) = B^i b^i C_4^i S[C_3^i \nu_0^i(t)] - 2b^i \nu_5^i(t) - (b^i)^2 \nu_2^i(t) \\
\dot{\nu}_6^i(t) = \nu_7^i(t) \\
\dot{\nu}_7^i(t) = A^i a^i S[\nu_1^i(t) - \nu_2^i(t)] - 2a^i \nu_7^i(t) - (a^i)^2 \nu_6^i(t)
\end{cases}
$$

where superscript i denotes the population under consideration (here, $i \epsilon \{1, 2\}$). This set of equations was solved by using the fourth-order Runge-Kutta integration method. At each population, the output signal, $y^i(t) = \nu_1^i(t) - \nu_2^i(t)$, is the summation of average excitatory and inhibitory PSPs in the pyramidal cell subpopulation and is analogous to a local field activity.

The Jansen model has been shown to produce a variety of LFP-like activities (Jansen

and Rit, 1995; Wendling et al., 2000). In this study, we considered the Jansen model in its oscillatory regime, which is obtained by using the set of parameters given in Table 1. As described in (Jansen and Rit, 1995), these parameters lead to the generation of alpha activity. However, it was found that a modification of some model parameters (i.e. the average synaptic gains, A and B, and rate constants, a and b) could make the model produce oscillations in the different EEG frequency bands (David and Friston, 2003). In this study, we were interested in theta oscillations. Consequently, we tuned the kinetics of the two subpopulations ($a^{-1} = 14\,\mathrm{ms}$; $b^{-1} = 28\,\mathrm{ms}$) so that the neuronal population model generates oscillatory activity in the theta band, according to the approach described in (David and Friston, 2003). An example of a simulated signal and its power spectral density is given in Figs. S5B and C.

References

David O, Friston KJ (2003) A neural mass model for MEG/EEG: coupling and neuronal dynamics. *Neuroimage* 20:1743–1755.

Jansen BH, Rit VG (1995) Electroencephalogram and visual evoked potential generation in a mathematical model of coupled cortical columns. *Biol Cybern* 73:357–366.

Wendling F, Bellanger JJ, Bartolomei F, Chauvel P (2000) Relevance of nonlinear lumped-parameter models in the analysis of depth-EEG epileptic signals. *Biol Cybern* 83:367–378.

Tab. 1: Physiological interpretation and values of model parameters (adapted from Wendling et al. (2000))

Parameter	Physiological interpretation	Value
A	Maximum amplitude of the average excitatory PSP	$3.25\,mV$
B	Maximum amplitude of the average inhibitory PSP	$22\,mV$
a	Rate constant of the average excitatory PSP	$100\,s^{-1}$
b	Rate constant of the average inhibitory PSP	$50\,s^{-1}$
C_1, C_2	Average numbers of synaptic contacts in the excitatory feedback loop	$C_1 = C, C_2 = 0.8\,C$ $(C = 135)$
C_3, C_4	Average numbers of synaptic contacts in the inhibitory feedback loop	$C_3 = 0.25\,C,$ $C_4 = 0.25\,C$
ν_0, e_0, r	Parameters of the sigmoid function	$\nu_0 = 6\,mV, e_0 = 2.5\,s^{-1},$ $r = 0.56\,mV^{-1}$